

---

---

# Whole-Body Distribution and Radiation Dosimetry of $^{11}\text{C}$ -(+)-PHNO, a $\text{D}_{2/3}$ Agonist Ligand

Romina Mizrahi, Pablo Rusjan, Irina Vitcu, Alvina Ng, Alan A. Wilson, Sylvain Houle, and Peter M. Bloomfield

Centre for Addiction and Mental Health, Toronto, Ontario, Canada

---

Using PET, we measured the whole-body distribution of  $^{11}\text{C}$ -(+)-PHNO ( $^{11}\text{C}$ -(+)-4-propyl-9-hydroxynaphthoxazine), a  $\text{D}_{2/3}$  agonist, as a function of time in adult subjects in order to determine the internal radiation dose. **Methods:** PET whole-body data were acquired after the injection of  $^{11}\text{C}$ -(+)-PHNO (~360 MBq) in 6 healthy subjects (3 male and 3 female). The PET acquisition duration was a maximum of 112.5 min, and 9 discrete time frames were obtained. After reconstruction of the emission data, 6 organs were identified in the images as exhibiting uptake above background levels. Regions of interest were delineated on these organs, and time-activity curves were generated. The time-activity curve data were corrected for the injected activity, specific organ density, and volume, from which normalized accumulated activities (previously known as residence times) were calculated. The normalized accumulated activities were then used with the software code OLINDA/EXM 1.1 to calculate the internal doses for the standard adult male and female models. **Results:** The mean effective dose was estimated to be  $4.5 \pm 0.3 \mu\text{Sv/MBq}$  when all subjects were included and the male model was applied for the dosimetry calculation, and the mean effective dose was estimated to be  $5.2 \pm 0.2 \mu\text{Sv/MBq}$  when the females were considered separately and the female model was applied for the calculation. The organ receiving the highest dose was the liver ( $17.9 \pm 3.9 \mu\text{Sv/MBq}$ ), followed by the kidneys ( $14.3 \pm 3.6 \mu\text{Sv/MBq}$ ) and the urinary bladder wall ( $13.5 \pm 3.7 \mu\text{Sv/MBq}$ ). **Conclusion:** The estimated radiation doses for  $^{11}\text{C}$ -(+)-PHNO are similar to those reported for other radiotracers labeled with  $^{11}\text{C}$ .  $^{11}\text{C}$ -(+)-PHNO may be used for multiple PET scans in the same subject and remain within regulatory guidelines.

**Key Words:** biodistribution; dosimetry; positron emission tomography; [ $^{11}\text{C}$ ](+)-PHNO;  $\text{D}_2$ ;  $\text{D}_3$

**J Nucl Med 2012; 53:1802-1806**

DOI: 10.2967/jnumed.112.105627

---

**T**he radiotracer  $^{11}\text{C}$ -(+)-PHNO,  $^{11}\text{C}$ -(+)-4-propyl-9-hydroxynaphthoxazine, is a  $\text{D}_{2/3}$  agonist (1) that binds with nanomolar affinity to  $\text{D}_2$  and  $\text{D}_3$  receptors, allowing for a prominent signal from the striatum and globus pallidus (2).

Unlike conventional  $\text{D}_{2/3}$  radiotracers, which are antagonists,  $\text{D}_{2/3}$  agonist radiotracers are desirable for 2 theoretic reasons: first, they may afford greater sensitivity in detecting changes in extracellular DA than antagonist compounds (3), and second, they may allow specific investigation of changes in  $\text{D}_2$  receptor agonist binding capacity. In addition,  $^{11}\text{C}$ -(+)-PHNO demonstrates greater than 10-fold higher affinity for  $\text{D}_3$  than for  $\text{D}_2$  (4) in vitro and an estimated higher affinity of approximately 20-fold in vivo (5).

The potential of  $^{11}\text{C}$ -(+)-PHNO as a radiotracer to image the  $\text{D}_2$  and  $\text{D}_3$  receptors in humans has already been shown (2,6-16). However, the radiation dosimetry estimates for those studies had been obtained by extrapolation from rat studies. This study provides updated dose estimates based on biodistribution data obtained directly in humans.

## MATERIALS AND METHODS

### Radiochemistry

The radiosynthesis of  $^{11}\text{C}$ -(+)-PHNO has been described in detail elsewhere (1). Purification by high-performance liquid chromatography and formulation gives radiochemically pure  $^{11}\text{C}$ -(+)-PHNO as a sterile, pyrogen-free solution suitable for human studies.

### Subjects

Six healthy volunteers (3 male and 3 female;  $64 \pm 8$  kg; age,  $29 \pm 9$  y) participated in this study. On the basis of history, physical examination (blood pressure, pulse, and respiration rate), electrocardiogram, urinalysis including drug screening, and a comprehensive blood chemistry screen, all subjects were free of current medical and psychiatric illness. These tests were performed before and after each  $^{11}\text{C}$ -(+)-PHNO scan. Our use of  $^{11}\text{C}$ -(+)-PHNO in human subjects was approved by the Centre for Addiction and Mental Health Research Ethics Board. All subjects gave written informed consent after all procedures were fully explained. Because the women were of child-bearing age, they had a urine pregnancy test just after they provided consent to the study and again immediately before the PET scan.

### PET Acquisition and Image Reconstruction

Studies were performed using a whole-body PET system, the Biograph HiRez XVI (Siemens Molecular Imaging), which measures radioactivity in 81 images, each with a thickness of 2.0 mm. The camera has both a CT and a PET component. The CT component is a 16-slice scanner and is used to acquire a minimal-dose CT scan from which the attenuation correction factors for the PET emission scan are calculated. The PET component has

---

Received Mar. 22, 2012; revision accepted Jun. 22, 2012.

For correspondence or reprints contact: Peter M. Bloomfield, Vivian M. Rakoff PET Centre, Research Imaging Centre, Centre for Addiction and Mental Health (CAMH), 250 College St., Toronto, Ontario, M5T 1R8, Canada.

E-mail: peter.bloomfield@camhpet.ca

Published online Sep. 11, 2012.

COPYRIGHT © 2012 by the Society of Nuclear Medicine and Molecular Imaging, Inc.

lutetium oxyorthosilicate crystal detectors, positioned in 3 rings of detector blocks, each ring consisting of 48 detectors. Each detector is arranged into  $13 \times 13$  crystals, each of which measures  $4 \times 4 \times 20$  mm. The axial and transaxial fields of view of the PET scanner are 16.2 and 58.5 cm, respectively, and the in-plane resolution of the scanner is approximately 4.6 mm in full width at half maximum (17).

Each subject was positioned supine and head first in the tomograph. This position was maintained for the duration of the acquisition using a thermoplastic mask for the head. Two additional restraining straps were wrapped around the subjects' chest and lower abdomen to minimize arm and body movement between the CT and the PET emission data acquisitions.

A CT scout view was acquired to determine the CT and PET axial scan length and confirm proper subject positioning. The acquisition field of view was defined from the scout view image to include top of head to mid thigh, resulting in 7, 8, or 9 bed positions per whole-body scan, depending on the height of the subject. Having defined the acquisition field of view, we acquired a minimal-dose CT scan. The CT total effective dose was estimated to be 4.5 mSv using the ImPACT CT Dosimetry Patient Calculator (<http://www.impactscan.org/ctdosimetry.htm>) with the following parameters: voltage, 140 kV; scan region, body; scan range, 1,015 mm, tube current, 60 mA; rotation time, 0.5 s; spiral pitch, 1.25; effective mAs, 24; collimation,  $16 \times 0.75 = 12$  mm). Using segmentation and scaling, we converted the CT images from Hounsfield units to a 511-keV  $\mu$ -map image, which was then forward projected to create the attenuation correction for the PET emission data.

A dynamic acquisition consisting of 9 whole-body scans was acquired in 3-dimensional sinogram mode (span, 11; ring difference, 27). Emission data were acquired for 15 s/bed position for scans 1 and 2, 30 s/bed position for scans 3 and 4, 60 s/bed position for scans 5 and 6, 120 s/bed position for scan 7, 180 s/bed position for scan 8, and 240 s/bed position for scan 9. One subject's dynamic acquisition consisted of 8 whole-body scans, where the final emission acquisition, scan 9 above, was not performed. The total acquisition duration was dependent on the number of bed positions per whole-body acquisition and was 87.5 min for a 7-bed-position scan, 100 min for an 8-bed-position scan, 112.5 min for a 9-bed-position scan, and 68 min for the patient with the 8 whole-body acquisitions. These acquisition durations do not include the time required to move the bed between either successive bed positions or whole-body acquisitions. The mean time between bed positions across all 6 studies was  $3.8 \pm 0.8$  s, and the corresponding mean time between the end of an acquisition and the start of successive whole-body acquisitions was  $15.0 \pm 1.4$  s.

$^{11}\text{C}(+)\text{-PHNO}$  was injected by hand as a slow bolus followed by a 20-mL saline flush via an intravenous catheter in the antecubital fossa. The injection was started 15 s before the start of acquisition. The 15-s delay accounted for circulation of the injectate through the body before arrival in the brain, at approximately the start of acquisition; that is, the first bed position. On completion of each whole-body acquisition, the bed returned to the first bed position and the next whole-body acquisition started.

After acquisition, the data were transferred to an off-line workstation for reconstruction of the whole-body images. The data for each 3-dimensional whole-body sinogram were normalized and corrected for attenuation and scatter before Fourier rebinning (18) to convert the 3-dimensional sinograms into 2-dimensional sinograms. The 2-dimensional sinograms were reconstructed into image

space twice: first, using an ordered-subset expectation maximization algorithm (19) with 4 iterations and 8 subsets, and second, using a direct inverse Fourier transform algorithm (20). After reconstruction, a gaussian filter of 5 mm in full width at half maximum in the 3 orthogonal planes was applied to the image. The images were calibrated to MBq/mL using a calibration factor determined before the acquisition. When all the bed positions had been reconstructed, including a correction for decay to the first bed position, a single whole-body image was constructed for each dynamic frame. Each reconstructed image had voxel dimensions of  $2.667 \times 2.667 \times 2.0$  mm ( $x,y,z$ ) and transverse plane dimensions of  $256 \times 256$  voxels ( $x,y$ ). The number of planes ( $z$ ) in the whole-body image is dependent on the number of bed positions acquired and was 429, 487, or 545 planes for a 7-, 8-, or 9-bed-position acquisition, respectively. The ordered-subset expectation maximization images were used for region-of-interest (ROI) placement because of the superior noise properties of iterative reconstructions, particularly in the chest and abdomen region, whereas the direct inverse Fourier transform images were used for dose assessment calculation because of the quantitative accuracy.

### Normalized Accumulated Activities

The ROIs were defined using Analyze (Biomedical Imaging Resource, Mayo Clinic College of Medicine). The ROIs selected were whole brain, left and right lung and kidney, liver, spleen, and bladder because these organs had a discernible activity concentration above the background level. The regions were traced on adjacent planes of the ordered-subset expectation maximization reconstructions in order to include the whole organ. The defined ROIs were then copied to the dynamic direct inverse Fourier transform whole-body series, and time-activity curves were extracted for each of the organs.

These time-activity curves were converted from MBq/mL to MBq/organ using the organ mass and density for the reference adult male or female (21), and normalized accumulated activities, previously referred to as residence time, were calculated for each organ using trapezoidal integration. It was assumed that after the end of the acquisition, the dominant process in the extrapolation of the time-activity curve to infinity was physical isotope decay of the injected ligand. A remainder fraction was calculated by subtracting the individual organ-normalized accumulated activities from the whole-body accumulated activity, which for  $^{11}\text{C}$  is 0.491 h.

For each subject, the normalized accumulated activities of each organ and the remainder were used in OLINDA/EXM 1.1 (22) to calculate the effective dose (using weighting factors as defined in ICRP publication 60 (23)) and the effective dose equivalent (using weighting factors as defined in ICRP publication 30 (24)) for the reference adult male. Independently, female values were calculated assuming the reference adult female organ densities and volumes and the model in OLINDA/EXM 1.1. The voiding bladder model, for either the male or female, was not assumed during the dosimetry calculation in OLINDA/EXM 1.1.

## RESULTS

The injected dose of  $^{11}\text{C}(+)\text{-PHNO}$  was  $356 \pm 21$  MBq, with a mass of  $1.70 \pm 0.66$   $\mu\text{g}$  and a specific activity at injection of  $1,561 \pm 545$  mCi/ $\mu\text{mol}$ . On the basis of patient reports, electrocardiogram, blood pressure, pulse, and respiration rate, the dose caused no pharmacologic effects during the scans.

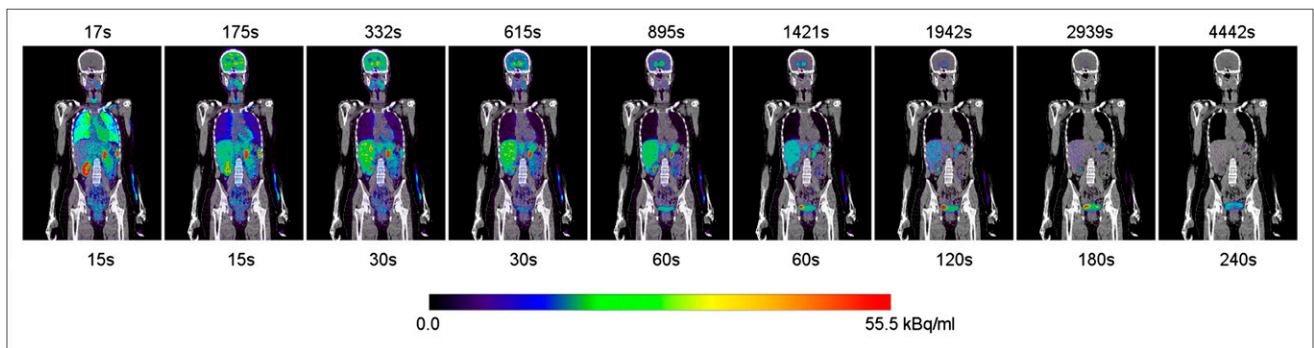


**FIGURE 1.**  $^{11}\text{C}$ -(+)-PHNO whole-body biodistribution over time for typical subject. PET (color scale) images are coregistered with subjects' CT image (gray scale). Time, in seconds, above each image is acquisition start time after injection of first bed position of whole-body image, whereas time, also in seconds, below each image is duration of each bed position in whole-body image. Image sequence is not decay-corrected to injection time; decay correction is applied only when each whole-body image is created from its individual-bed-position images.

A typical  $^{11}\text{C}$ -(+)-PHNO biodistribution is shown in Figure 1. All subjects had a distribution of radioactivity that was expected from the known densities of  $\text{D}_{2/3}$  in the body and in accordance with other  $\text{D}_{2/3}$  agonist radioligands (25–27).

Because of the difference in acquisition timing between the 6 subjects, the normalized organ activity was either interpolated or extrapolated onto a common temporal frame, calculated from the mean mid-frame time for the 6 subjects, after which the organ mean and SD across the 6 subjects were calculated as shown in Figure 2. The lungs presented the highest uptake, with a peak of  $27.8\% \pm 11.6\%$  (mean  $\pm$  SD) of the injected activity occurring during the first frame of acquisition after injection, followed by the liver ( $19.0\% \pm 6.5\%$ ) during the third frame of measurement ( $\sim 6$  min after injection). Activity in the brain peaked in the second frame ( $\sim 3$  min after injection), with a maximum of  $8.0\% \pm 2.6\%$  of the injected activity; kidneys and spleen peaked earlier in the first frame, with  $4.5\% \pm 0.6\%$  and  $2.2\% \pm 0.3\%$  of the injected activity, respectively. The time-activity curve of the bladder peaked at around 30 min after injection, with 1.7% of the injected activity. At the end of acquisition the liver had 1.2% of the injected dose, the maximum of all the organs.

The normalized accumulated activities of organs estimated by this method are listed in Table 1. The first column shows the values calculated assuming standard male mass and density of the organs of the 6 subjects regardless

of sex (21) and the second takes into account only the 3 female subjects and assumes standard mass for female organs (21). Table 2 shows the estimated radiation doses calculated with OLINDA/EXM 1.1. The effective dose was  $4.5 \pm 0.3 \mu\text{Sv}/\text{MBq}$  using the standard adult “hermaphrodite” male model and increased to  $5.2 \pm 0.2 \mu\text{Sv}/\text{MBq}$  when only females were considered and the standard female model used.

The largest absorbed dose was in the liver ( $17.9 \pm 3.9 \mu\text{Gy}/\text{MBq}$ ), followed by the kidneys ( $14.3 \pm 3.6 \mu\text{Gy}/\text{MBq}$ ) and urinary bladder wall ( $13.5 \pm 3.7 \mu\text{Gy}/\text{MBq}$ ).

## DISCUSSION

The human temporal biodistribution of  $^{11}\text{C}$ -(+)-PHNO radioactivity concentration was measured using a PET/CT scanner, and the internal radiation doses were estimated. We found that a PET/CT tomograph can be used effectively to acquire the tissue concentration data for dosimetry calculations. The estimated effective doses ( $4.5 \pm 0.3 \mu\text{Sv}/\text{MBq}$ ) for a standard adult hermaphrodite male model with OLINDA/EXM 1.1 are slightly lower than those previously extrapolated from rat studies ( $5.1 \mu\text{Sv}/\text{MBq}$ ) and similar to or lower than other  $^{11}\text{C}$ -labeled radioligands. Therefore, when a bolus of 356 MBq of  $^{11}\text{C}$ -(+)-PHNO is injected, the typical effective dose would be 1.6 mSv, and the most affected organ would be the liver at 6.4 mGy. The female model applied to the female subjects was investigated to

**FIGURE 2.** Mean organ uptake (expressed as percentage of injected dose) for all 6 subjects over time. Vertical bars represent SD, and data are not decay-corrected to time 0.

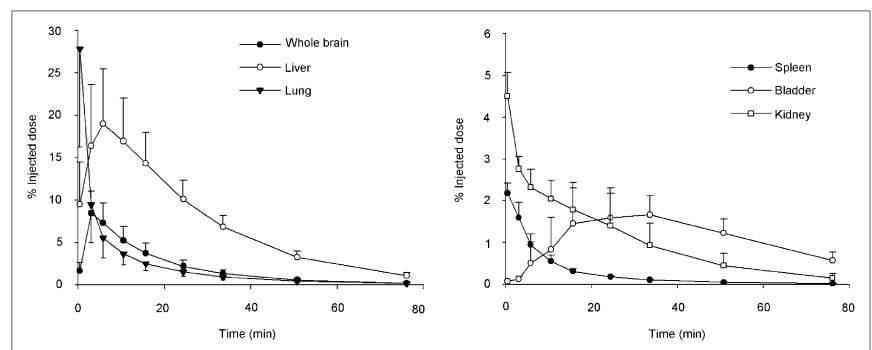


**TABLE 1**

Normalized Accumulated Activity Measured Assuming Organ Volume for Standard Male and Female

Organ	All subjects ( <i>n</i> = 6) as males	Females ( <i>n</i> = 3) as females
Whole brain	0.027 ± 0.007	0.029 ± 0.005
Lung	0.027 ± 0.009	0.027 ± 0.007
Liver	0.102 ± 0.024	0.073 ± 0.011
Spleen	0.003 ± 0.001	0.003 ± 0.000
Kidneys	0.014 ± 0.004	0.014 ± 0.005
Bladder	0.017 ± 0.005	0.011 ± 0.003
Remainder	0.300 ± 0.025	0.333 ± 0.009

Data are organ MBq·h divided by injected MBq (mean ± SD).

provide insight into whether the sexes should be differentiated when dosimetry calculations are performed. The female biodistribution data used with the female adult phantom gave an effective dose that was 15.6% higher in this subset (*n* = 3) than when the full set (*n* = 6) of subjects was used with the hermaphrodite male model. Though the sample size was small, the female model effective dose did not change the maximum number of scans per year, but the findings do suggest that when human dosimetry is calculated, the data should be investigated separately for the sexes.

For our study, using a whole-body PET/CT Biograph HiRez XVI, the effective dose of the minimal-dose CT scan for the whole-body adult male was estimated to be 4.5 mSv, a dose significantly higher than the dose from <sup>11</sup>C-(+)-PHNO. However, the effective doses of a CT scan used to provide attenuation data for a neurologic PET scan can be reduced to 0.07 mSv (also estimated using the IMPACT CT Dosimetry Patient Calculator with the following parameters: voltage, 60 kV; scan region, brain; rotation time, 0.5 s; spiral pitch, 1.25, effective mAs, 23; and collimation, 16 × 0.75 = 12 mm.). Therefore, with these parameters, the CT dose is markedly reduced compared with about 2.5 mSv for a typical diagnostic neurologic CT scan.

Several assumptions have been made to allow for an estimation of the effective dose of <sup>11</sup>C-(+)-PHNO to be calculated. First, we assumed that in the interleaved planes of the whole-body images, the kinetics of the ligand were the same and that the main effect was decay. Although this is obviously not the case during the early phases of ligand delivery, the effect was minimized when small acquisition durations were chosen for this part of the scan. An attempt was made during the definition of the acquisition length to position the center of the larger organs, such as liver, brain, and heart, at or toward the center of a single bed position. Alternatively, the ROI could be described on the individual bed position images, thereby avoiding this effect. Second, we assumed that the volume of the bladder was constant for the duration of the acquisition. This was clearly not the case, as radiotracer uptake by the bladder grew in size over

the course of the acquisition as the ligand was excreted from the blood into the urine. A better solution would be to describe a volume ROI that increases as the bladder grows over the duration of the acquisition, with the smallest volume for the early time frames. However, for the sake of consistency with previously reported dosimetry studies, this method was not used.

Also, although radioactivity was seen in the vertebrae, delineation of the marrow in the lumbar vertebrae with regions of interest and extrapolation to the total-body marrow was deemed somewhat arbitrary and error-prone, and the marrow activity was included in the remainder-of-body fraction in the final analysis. Inclusion or exclusion of the marrow as a distinct organ affected the dose estimates minimally—significantly less than did intersubject variability.

## CONCLUSION

The estimated effective adult radiation dose for <sup>11</sup>C-(+)-PHNO derived from human biodistribution data was

**TABLE 2**

Organ Dose as Calculated by OLINDA/EXM 1.1 for Standard Adult Hermaphrodite Male Model as Applied to All 6 Subjects and Standard Female Model as Applied Only to the 3 Female Subjects

Parameter	SAHMM	SAFM
Organ dose (μGy/MBq)		
Adrenals	3.5 ± 0.1	4.3 ± 0.1
Brain	6.4 ± 1.7	8.2 ± 1.2
Breasts	2.0 ± 0.1	2.6 ± 0.0
Gallbladder wall	4.4 ± 0.4	4.8 ± 0.2
Lower large intestine wall	2.4 ± 0.2	3.2 ± 0.1
Small intestine	2.6 ± 0.1	3.2 ± 0.1
Stomach wall	2.6 ± 0.1	3.4 ± 0.0
Upper large intestine wall	2.7 ± 0.1	3.5 ± 0.1
Heart wall	2.9 ± 0.0	3.7 ± 0.1
Kidneys	14.3 ± 3.6	15.8 ± 4.5
Liver	17.9 ± 3.9	17.4 ± 2.4
Lungs	8.2 ± 2.2	10.1 ± 2.3
Muscle	2.2 ± 0.1	2.9 ± 0.1
Ovaries	2.5 ± 0.2	3.3 ± 0.1
Pancreas	3.4 ± 0.1	4.2 ± 0.1
Red marrow	2.1 ± 0.1	2.7 ± 0.0
Osteogenic cells	3.1 ± 0.2	4.4 ± 0.1
Skin	1.7 ± 0.1	2.3 ± 0.0
Spleen	6.4 ± 0.8	7.6 ± 0.5
Testes	2.0 ± 0.1	—
Thymus	2.2 ± 0.1	3.1 ± 0.1
Thyroid	2.1 ± 0.1	2.6 ± 0.1
Urinary bladder wall	13.5 ± 3.7	12.8 ± 3.2
Uterus	2.8 ± 0.2	3.5 ± 0.2
Total body	2.9 ± 0.0	3.6 ± 0.0
Effective dose (μSv/MBq)		
Effective dose equivalent	5.8 ± 0.4	6.7 ± 0.2
Effective dose	4.5 ± 0.3	5.2 ± 0.2

SAHMM = standard adult hermaphrodite male model; SAFM = standard female model.

4.5 ± 0.3 μSv/MBq, or 1.6 mSv for a typical injection of 370 MBq of <sup>11</sup>C-(+)-PHNO, and was slightly higher in women. The liver, which received the highest radiation dose (6.4 mSv), was well below the dose guideline (50 mSv) as reported for that organ by the Food and Drug Administration (title 21 of *Code of Federal Regulations* part 361.1; <http://www.accessdata.fda.gov/scripts/cdrh/cfdocs/cfcfr/CFRSearch.cfm?FR=361.1>). The radiation dose estimates were low enough to allow repeated scans within a calendar year in the same subject and remain within regulatory guidelines for internal radiation dose.

## DISCLOSURE STATEMENT

The costs of publication of this article were defrayed in part by the payment of page charges. Therefore, and solely to indicate this fact, this article is hereby marked “advertisement” in accordance with 18 USC section 1734.

## ACKNOWLEDGMENTS

We thank Armando Garcia, Winston Stableford, and Min Wong for their excellent technical assistance. This study was supported by Canada Foundation for Innovation and the Ontario Ministry of Research and Innovation and in part by a New Investigator Award from CIHR and an Ontario Mental Health Foundation New Investigator Fellowship. No other potential conflict of interest relevant to this article was reported.

## REFERENCES

- Wilson AA, McCormick P, Kapur S, et al. Radiosynthesis and evaluation of [<sup>11</sup>C]-(+)-4-propyl-3,4,4a,5,6,10b-hexahydro-2H-naphtho[1,2-b][1,4]oxazin-9-ol as a potential radiotracer for in vivo imaging of the dopamine D2 high-affinity state with positron emission tomography. *J Med Chem.* 2005;48:4153–4160.
- Willeit M, Ginovart N, Kapur S, et al. High-affinity states of human brain dopamine D2/3 receptors imaged by the agonist [<sup>11</sup>C]-(+)-PHNO. *Biol Psychiatry.* 2006;59:389–394.
- Narendran R, Mason NS, Laymon CM, et al. A comparative evaluation of the dopamine D<sub>2/3</sub> agonist radiotracer [<sup>11</sup>C](-)-N-propyl-norapomorphine and antagonist [<sup>11</sup>C]raclopride to measure amphetamine-induced dopamine release in the human striatum. *J Pharmacol Exp Ther.* 2010;333:533–539.
- Parker C, Clarke K, Gee AD, Gee A, Rabiner E. In vitro characterisation of the high affinity D2/D3 dopamine agonist (+)PhNO [abstract]. *Neuroimage.* 2006;31(suppl 2):T29.
- Gallezot J, Beaver J, Nabulsi N, et al. [<sup>11</sup>C]-PHNO studies in rhesus monkey: In vivo affinity for D2 and D3 receptors and dosimetry [abstract]. *J Nucl Med.* 2009;50(suppl 2):157P.
- Boileau I, Guttman M, Rusjan P, et al. Decreased binding of the D3 dopamine receptor-preferring ligand [<sup>11</sup>C]-(+)-PHNO in drug-naive Parkinson's disease. *Brain.* 2009;132:1366–1375.
- Ginovart N, Galineau L, Willeit M, et al. Binding characteristics and sensitivity to endogenous dopamine of [<sup>11</sup>C]-(+)-PHNO, a new agonist radiotracer for imaging the high-affinity state of D2 receptors in vivo using positron emission tomography. *J Neurochem.* 2006;97:1089–1103.
- Graff-Guerrero A, Mamo D, Shammi CM, et al. The effect of antipsychotics on the high-affinity state of D2 and D3 receptors: a positron emission tomography study with [<sup>11</sup>C]-(+)-PHNO. *Arch Gen Psychiatry.* 2009;66:606–615.
- Mizrahi R, Agid O, Borlido C, et al. Effects of antipsychotics on D3 receptors: a clinical PET study in first episode antipsychotic naive patients with schizophrenia using [<sup>11</sup>C]-(+)-PHNO. *Schizophr Res.* 2011;131:63–68.
- Mizrahi R, Houle S, Vitcu I, Ng A, Wilson AA. Side effects profile in humans of <sup>11</sup>C-(+)-PHNO, a dopamine D<sub>2/3</sub> agonist ligand for PET. *J Nucl Med.* 2010;51:496–497.
- Narendran R, Slifstein M, Guillin O, et al. Dopamine (D2/3) receptor agonist positron emission tomography radiotracer [<sup>11</sup>C]-(+)-PHNO is a D3 receptor preferring agonist in vivo. *Synapse.* 2006;60:485–495.
- Rabiner EA, Laruelle M. Imaging the D3 receptor in humans in vivo using [<sup>11</sup>C]-(+)-PHNO positron emission tomography (PET). *Int J Neuropsychopharmacol.* 2010;13:289–290.
- Searle G, Beaver JD, Comley RA, et al. Imaging dopamine D3 receptors in the human brain with positron emission tomography, [<sup>11</sup>C]PHNO, and a selective D3 receptor antagonist. *Biol Psychiatry.* 2010;68:392–399.
- Sholtolt P, Tziortzi AC, Searle GE, et al. Within-subject comparison of [<sup>11</sup>C]-(+)-PHNO and [<sup>11</sup>C]raclopride sensitivity to acute amphetamine challenge in healthy humans. *J Cereb Blood Flow Metab.* 2012;32:127–136.
- Tziortzi AC, Searle GE, Tzimopoulou S, et al. Imaging dopamine receptors in humans with [<sup>11</sup>C]-(+)-PHNO: dissection of D3 signal and anatomy. *Neuroimage.* 2011;54:264–277.
- Willeit M, Ginovart N, Graff A, et al. First human evidence of d-amphetamine induced displacement of a D<sub>2/3</sub> agonist radioligand: a [<sup>11</sup>C]-(+)-PHNO positron emission tomography study. *Neuropsychopharmacology.* 2008;33:279–289.
- Brambilla M, Secco C, Dominietto M, Matheoud R, Sacchetti G, Ingelse E. Performance characteristics obtained for a new 3-dimensional lutetium oxyorthosilicate-based whole-body PET/CT scanner with the National Electrical Manufacturers Association NU 2-2001 standard. *J Nucl Med.* 2005;46:2083–2091.
- Defrise M, Kinahan PE, Townsend DW, Michel C, Sibomana M, Newport DF. Exact and approximate rebinning algorithms for 3-D PET data. *IEEE Trans Med Imaging.* 1997;16:145–158.
- Hudson HM, Larkin RS. Accelerated image reconstruction using ordered subsets of projection data. *IEEE Trans Med Imaging.* 1994;13:601–609.
- Hamill J. Evaluating a frequency-space SPECT reconstruction algorithm. *Proc Opt Engineering Midwest.* 1995;SPIE vol. 2622:785–791.
- Basic anatomical and physiological data for use in radiological protection: reference values—a report of age- and gender-related differences in the anatomical and physiological characteristics of reference individuals. ICRP Publication 89. *Ann ICRP.* 2002;32:5–265.
- Stabin MG, Sparks RB, Crowe E. OLINDA/EXM: the second-generation personal computer software for internal dose assessment in nuclear medicine. *J Nucl Med.* 2005;46:1023–1027.
- ICRP. Recommendations of the International Commission on Radiological Protection. ICRP publication 60. *Ann ICRP.* 1990;21:1991.
- ICRP. Limits for intakes of radionuclides by workers. ICRP publication 30 (part 1). *Ann ICRP.* 1979;2.
- Laymon CM, Mason NS, Frankle WG, et al. Human biodistribution and dosimetry of the D2/3 agonist <sup>11</sup>C-N-propyl-norapomorphine (<sup>11</sup>C-NPA) determined from PET. *J Nucl Med.* 2009;50:814–817.
- Seneca N, Skinbjerg M, Zoghbi SS, et al. Kinetic brain analysis and whole-body imaging in monkey of [<sup>11</sup>C]MNPDA: a dopamine agonist radioligand. *Synapse.* 2008;62:700–709.
- Slifstein M, Hwang DR, Martinez D, et al. Biodistribution and radiation dosimetry of the dopamine D2 ligand <sup>11</sup>C-raclopride determined from human whole-body PET. *J Nucl Med.* 2006;47:313–319.